The Journal of Chemical Physics

Understanding the structure of complex multidimensional wave functions. A case study of excited vibrational states of ammonia

Cite as: J. Chem. Phys. **154**, 144306 (2021); https://doi.org/10.1063/5.0043946
Submitted: 12 January 2021 . Accepted: 23 March 2021 . Published Online: 09 April 2021

Jan Šmydke, and Attila G. Császár

The Journal of Chemical Physics ARTICLE scitation.org/journal/jcp

Understanding the structure of complex multidimensional wave functions. A case study of excited vibrational states of ammonia

Cite as: J. Chem. Phys. 154, 144306 (2021); doi: 10.1063/5.0043946
Submitted: 12 January 2021 • Accepted: 23 March 2021 •
Published Online: 9 April 2021

Jan Šmydke[1,a] and Attila G. Császár[2]

AFFILIATIONS

[1] Department of Radiation and Chemical Physics, Institute of Physics CAS, Na Slovance 1999/2, 18221 Praha 8, Czech Republic
[2] MTA-ELTE Complex Chemical Systems Research Group and Laboratory of Molecular Structure and Dynamics, Institute of Chemistry, ELTE Eötvös Loránd University, H-1117 Budapest, Pázmány Péter Sétány 1/A, Hungary

Note: This paper is part of the JCP Special Topic on Quantum Dynamics with *Ab Initio* Potentials.
[a] **Author to whom correspondence should be addressed:** jan.smydke@gmail.com

ABSTRACT

Generalization of an earlier reduced-density-matrix-based vibrational assignment algorithm is given, applicable for systems exhibiting both large-amplitude motions, including tunneling, and degenerate vibrational modes. The algorithm developed is used to study the structure of the excited vibrational wave functions of the ammonia molecule, $^{14}NH_3$. Characterization of the complex dynamics of systems with several degenerate vibrations requires reconsidering the traditional degenerate-mode description given by vibrational angular momentum quantum numbers and switching to a symmetry-based approach that directly predicts state degeneracy and uncovers relations between degenerate modes. Out of the 600 distinct vibrational eigenstates of ammonia obtained by a full-dimensional variational computation, the developed methodology allows for the assignment of about 500 with meaningful labels. This study confirms that vibrationally excited states truly have modal character recognizable up to very high energies even for the non-trivial case of ammonia, a molecule which exhibits a tunneling motion and has two two-dimensional normal modes. The modal characteristics of the excited states and the interplay of the vibrational modes can be easily visualized by the reduced-density matrices, giving an insight into the complex modal behavior directed by symmetry.

I. INTRODUCTION

It is a common argument against sophisticated quantum-chemical computations, such as the variational ones, which are widely performed in the fourth age of quantum chemistry,[1] that they provide a lot of data, some in the form of wave functions, but only limited understanding. To most chemists, an approximate characterization of the (ro)vibrational dynamics of molecular systems requires that certain descriptors are attached to the computed wave functions. These descriptors are most often quantum numbers arising from simple models.[2] Aside from the use of *good quantum numbers*, the understanding of the internal structure of multidimensional excited-state wave functions requires the use of approximate quantum numbers. When the emphasis is on physical meaning and interpretation, the descriptors are commonly associated with the character of a dominant component of the given state expanded in a particular basis set.[3] For example, the $1s^1 2s^1$ electronic excited state of a helium atom is distinguished by its dominating $1s^1 2s^1$ two-electron full configuration interaction (FCI) basis vector, although this state also has many other non-zero FCI basis contributions. Nevertheless, a general excited state may decompose to more than one dominant basis vector or the composition of the state may even be evenly distributed over the whole basis-set space, not giving a particular vector or a selection of vectors' significant preference over the others.

In such ambiguous cases, the question arises naturally whether one could still associate a given state of interest with a unique physical meaning other than just energy and overall symmetry

that come naturally from the quantum-chemical computation. One may also ask whether changes in the multidimensional basis could turn more states into those exhibiting a dominant contribution. Such a smart transformation prescription, however, is not known generally.

Apart from the state composition, a general and unique characteristic of multidimensional excited states of quantum systems is the number of the wave-function nodes in each of the systems' modes of motion. The given excited state is then associated with a set of modal quantum numbers, regardless of the particular basis set used. This approach proved to be a practical way to label excited rovibrational states of small molecules.[2] As we have shown earlier[4,5] for vibrational wave functions resulting from sophisticated variational computations, the individual mode excitations tend to have a characteristic and distinguishable density by means of the reduced-density matrices (*vide infra*) that are also easier to handle than a bare multidimensional wave function. Nevertheless, the density, as a function of coordinates, and the position of the nodes may not always match with the underlying modal basis functions. The deviation can be significant when several modes interact, and in such cases, the bare basis-set-decomposition method may fail to characterize the state. A suitable choice of the modes of motion and the ability to count the number of nodes in each mode of complicated multidimensional wave functions are key to the general and practical characterization of excited states. It is, however, not well understood how many states can be unambiguously assigned by this approach.

In this paper, we examine vibrational excited states of the ammonia molecule ($^{14}NH_3$), a system exhibiting nontrivial modal structure. In particular, ammonia is a symmetric-top molecule, it has two twofold-degenerate vibrational modes, and it exhibits a large-amplitude internal motion (tunneling). We demonstrate that by using a simple coordinate system that intuitively mimics the harmonic vibrational modes of ammonia and with the help of reduced-density matrices for reading out the number of modal nodes, we can unambiguously assign hundreds of vibrationally excited states of $^{14}NH_3$. We compare our results to the recent state-of-the-art rovibrational line and energy level list of ammonia[6] that provides a quick and fully automatic assignment of all states of interest based on the dominant basis-set component, but the assignments may not always be accurate.

The rest of this paper is structured as follows. Section II discusses a few theoretical aspects of the vibrational assignment process together with the treatment of systems possessing degenerate modes, which is essential for the correct description of the vibrations of ammonia. Section III describes the technical details of variational vibrational wave-function computations. Section IV shows, explains, and discusses the main results of this paper. The most important conclusions of the present study are summarized in Sec. V.

II. THEORY

A. Multidimensional structure of vibrational states

Understanding the dynamical behavior of multidimensional quantum systems may start with a model in which individual degrees of freedom (dof) in the ground state are least coupled or can be considered semi-independent. A well-known example from another field is the Hartree–Fock approximation[7] of electronic-structure theory, where the individual electrons are moving independently in the averaged field of the other electrons and the nuclei. This model is necessarily far from being perfect; the motion of the electrons is not truly independent as each electron contributes to the self-consistent field by which all the electrons are driven. Nevertheless, the individual one-electron functions, the so-called orbitals, have been playing, for many decades, a crucial role in the qualitative understanding of the structure and reactivity of molecules, and they also form the foundation of correlated wave-function expansions of the ground and of the excited electronic states.

Similarly, the harmonic oscillator model[8] of the vibrations of polyatomic molecules constructs the ground and excited vibrational states by combining independent (the so-called normal) modes of vibrations, as can be seen from the harmonic oscillator energy formula for the ith vibrationally excited state,

$$E_i = \sum_m v_m^{(i)} \varepsilon_m + \mathrm{ZPVE}, \tag{1}$$

where the index m runs over all vibrational modes, ε_m and $v_m^{(i)}$ are the energy and the excitation quantum number of the mth mode, and ZPVE stands for zero-point vibrational energy. The modes are linear combinations of all the nuclear dofs and are made independent due to the quadratic nature of the vibrational potential in the harmonic approximation. The decomposition of vibrational states into modes of the harmonic oscillator model is still the *de facto* standard description of molecular vibrations, and it is generally accepted and used by practitioners of the field.

Apart from the anharmonic nature of potential energy surfaces (PESs),[9–11] which results in mode coupling and considerable shifting of the harmonic energy levels, when studying higher vibrationally excited states or when dealing with semi-rigid systems with several shallow potential energy wells, the strategy of combining the independent normal modes, constrained to a single minimum by definition, quickly becomes inappropriate. In some cases, it is preferable to replace the normal-mode description by a local-mode treatment, for example, for the vibrations of the heavier congeners of water.[12] For semi-rigid molecules, splitting of energy levels due to tunneling between symmetrically equivalent configurations (such as the two minima of ammonia linked by an umbrella-like nuclear motion) makes the spectra more complex and the normal-mode picture inappropriate, especially for higher excitations.

If the model of a normal-mode combination fails quantitatively and even qualitatively for a general polyatomic system, the question arises whether it is still reasonable and possible to characterize highly excited multidimensional wave functions by means of combinations of "modes." No matter what the modal degrees of freedom are and how strongly coupled they become in various states, the modes should retain a more-or-less intact character for portions of the energy spectrum so that they are clearly distinguishable and the modal understanding of the excited states remains meaningful.

Due to their convenience, modal combinations are routinely used in the qualitative description of vibrational states, although the

assignment is often cumbersome and tends to become inaccurate as the excitation increases. There are a variety of techniques of vibrational assignment. They range from energy decomposition, based on or similar to Eq. (1), finite basis representation (FBR)[13] and other[2] decomposition schemes based on the wave-function overlap with modal basis functions and similar yet conceptually different vibrational configuration interaction vector decompositions,[14] and various expectation-value-based[2] or even perturbative approaches[15,16] to direct inspection of two-dimensional (2D) cuts of vibrational wave functions. The last technique mentioned can provide a valuable visual insight into the nodal structure of vibrations and the interplay of modes. By counting the number of wave-function nodes in each of the vibrational modes, one can directly assign modal quantum numbers that characterize the polyatomic vibrational state. Practically, however, this approach has a limited range of applicability, and it is mainly useful to states with pure bending or stretching character and only to low-lying states.[17,18] For states excited by more than just a few quanta or states with strongly coupled modes, the nodal information from the 2D plots is mostly not legible.[4,19] Moreover, the number of 2D plots that needs to be inspected rises as $\binom{n}{2}$, where n stands for the number of vibrational degrees of freedom, which is not easy to handle manually even for a few-atomic system.

In our recent study about the nuclear dynamics of the vinyl radical,[4] we came up with an alternative way of visualizing the vibrational wave-function modes by means of reduced-density matrices (RDMs) along selected internal coordinates. While this was not the first use of RDM in the context of molecular vibrations, we extended its applicability much further than a simple 2D visual characterization tool.[20] Our RDM approach proved to be advantageous over the use of 2D wave-function cuts in several respects. The nodal structure of a particular vibrational mode is far more legible with RDM than with wave-function cuts, and as a result, many more states can be assigned. In contrast to wave-function cuts, RDMs need considerably less data generated and inspected. Moreover, RDMs do not depend on a reference vibrational configuration. It also turned out that each modal excitation exhibited a peculiar density pattern that could be used for identifying modal excitations in a semi-automatic way; this has already been successfully applied to the assignment of many vibrational states of the water molecule.[5] Although the RDMs of particular modal excitations tend to retain their characteristic shapes throughout a large portion of the energy spectrum, heavily coupled modes can deviate from the regular RDM shapes significantly. Nevertheless, such cases tend to be still well assignable by using a simple logic, and their irregular density shape, then, serves as a specific pattern for similarly coupled modes in other excited states. By using various RDM types, one can decode complicated vibrational structures from different contexts, which helps distinguishing states that look similar, as demonstrated on the vibrational states of ammonia during this work.

Since the RDM technique proved successful in correctly identifying modal excitations for a considerable number of states, we can conjecture that the view of vibrationally excited states as virtually decomposable to individually excited vibrational modes is truly meaningful for a much higher number of states than suggested by other approaches. We do not imply that there is a clear energy decomposition into modal contributions, but rather that for a given set of vibrational modes, the excited state can be decomposed into individual, distinguishable mode excitations with the characteristic nodal structure. In contrast to the method of wave-function overlap with modal basis functions, which can yield incorrect modal quantum numbers, the RDM approach allows for a direct visual mode assessment even in cases when the modal density shape strongly deviates from the basis functions.

It needs to be stressed that the success of the modal description may heavily depend on the clever definition of the vibrational modes and the underlying coordinate system. In the molecules studied so far, we associated the vibrational modes with intuitively chosen coordinates, expecting particular vibrational motions. Even though they were successful choices, it is not yet clear how to select the most suitable set of coordinates systematically and whether a completely different set of modes/coordinates would lead to equivalent or inferior results and would still provide an intuitive physical insight. One question, going beyond the scope of this work, thus, remains open: How far one can reach in the characterization of a vibrational spectrum by using just a single set of vibrational modes?

B. Reduced-density matrices and vibrational labeling

First, let us briefly summarize the definitions of various types of reduced-density matrices that come handy for inspecting multidimensional wave functions. Suppose that we have an N-dimensional vibrational wave function,

$$|\Psi_{\mathrm{vib}}\rangle \equiv \Psi(q_1, \ldots, q_N). \tag{2}$$

Then, the one-mode reduced-density matrix (1RDM) is defined as

$$\begin{aligned}\Gamma_1(q_i', q_i) = \int \mathrm{d}q_1 \ldots \mathrm{d}q_{i-1}\mathrm{d}q_{i+1} \ldots \mathrm{d}q_N \\ \times \Psi^*(q_1, \ldots, q_{i-1}, q_i', q_{i+1}, \ldots, q_N) \\ \times \Psi(q_1, \ldots, q_{i-1}, q_i, q_{i+1}, \ldots, q_N).\end{aligned} \tag{3}$$

We can view the 1RDM as a two-dimensional quantity for a single vibrational coordinate q_i, obtained after integrating out all the remaining vibrational degrees of freedom. Taking only the diagonal elements of 1RDM, we end up with the diagonal one-mode reduced-density matrix,

$$\begin{aligned}\Gamma_1^{\mathrm{D}}(q_i) \equiv \Gamma_1(q_i, q_i) = \int \mathrm{d}q_1 \ldots \mathrm{d}q_{i-1}\mathrm{d}q_{i+1} \ldots \mathrm{d}q_N \\ \times \Psi^*(q_1, \ldots, q_N)\Psi(q_1, \ldots, q_N),\end{aligned} \tag{4}$$

which stands as a true wave-function density for the given coordinate q_i.

Similarly, one can define a two-mode reduced-density matrix (2RDM) as a four-dimensional quantity,

$$\begin{aligned}&\Gamma_2(q_i', q_j', q_i, q_j) \\ &\quad = \int \mathrm{d}q_1 \ldots \mathrm{d}q_{i-1}\mathrm{d}q_{i+1} \ldots \mathrm{d}q_{j-1}\mathrm{d}q_{j+1} \ldots \mathrm{d}q_N \\ &\qquad \times \Psi^*(q_1, \ldots, q_{i-1}, q_i', q_{i+1}, \ldots, q_{j-1}, q_j', q_{j+1}, \ldots, q_N) \\ &\qquad \times \Psi(q_1, \ldots, q_{i-1}, q_i, q_{i+1}, \ldots, q_{j-1}, q_j, q_{j+1}, \ldots, q_N).\end{aligned} \tag{5}$$

The diagonal elements of 2RDM can be viewed as a true two-dimensional density,

$$\begin{aligned}\Gamma_2^{\mathrm{D}}(q_i,q_j) &\equiv \Gamma_2(q_i,q_j,q_i,q_j)\\ &= \int \mathrm{d}q_1 \ldots \mathrm{d}q_{i-1}\mathrm{d}q_{i+1} \ldots \mathrm{d}q_{j-1}\mathrm{d}q_{j+1} \ldots \mathrm{d}q_N\\ &\quad \times \Psi^*(q_1,\ldots,q_N)\Psi(q_1,\ldots,q_N). \end{aligned} \tag{6}$$

We suggest to look at this quantity as a convenient resolution of the $\Gamma_1^{\mathrm{D}}(q_i)$ density in one additional dimension. Γ_2^{D}s greatly improve the understanding of the characteristics of the vibrational states, and they are also necessary for the description of degenerate or otherwise coupled vibrational modes.

In the same manner, one can construct even higher-order reduced-density matrices. The high-rank tensor quantities are, however, difficult to visualize, and their storage and manipulation can quickly become intractable. It is, therefore, preferable to restrict the analysis to low-order RDMs, whenever possible. This recommendation was followed in our previous studies.[4,5] Nevertheless, for the present study, we found it necessary to also use three-dimensional $\Gamma_3^{\mathrm{D}}(q_i,q_j,q_k)$ diagonal densities,

$$\begin{aligned}\Gamma_3^{\mathrm{D}}(q_i,q_j,q_k) &\equiv \Gamma_3(q_i,q_j,q_k,q_i,q_j,q_k)\\ &= \int \mathrm{d}q_1 \ldots \mathrm{d}q_{i-1}\mathrm{d}q_{i+1} \ldots \mathrm{d}q_{j-1}\mathrm{d}q_{j+1} \ldots\\ &\quad \times \mathrm{d}q_{k-1}\mathrm{d}q_{k+1} \ldots \mathrm{d}q_N\\ &\quad \times \Psi^*(q_1,\ldots,q_N)\Psi(q_1,\ldots,q_N). \end{aligned} \tag{7}$$

In our study of the vinyl radical,[4] we used only the diagonal densities $\Gamma_1^{\mathrm{D}}(q_i)$ and $\Gamma_2^{\mathrm{D}}(q_i,q_j)$, and the assignment of the states was performed exclusively by their visual assessment. It was nevertheless a step forward compared to direct wave-function inspection as the two-dimensional wave-function cuts were very complex and extremely confusing, except for the few lowest-energy states. With the help of the densities, which effectively integrate out misleading structural details originating from other vibrational modes, we could clearly count the nodes in any vibrational mode as strongly pronounced kinks in the density profiles. Furthermore, we observed that each individual mode excitation had a very characteristic density shape, which did not change in the states of the same modal quantum number. Only states with expected strong coupling between particular modes exhibited deviations from the otherwise very regular density pattern. These results were, at the same time, surprising and encouraging for us to pursue the RDM technique further. Not only were we able to assign an order of magnitude more vibrational states with relative ease and confidence than with other methods, but it also suggested that the modal understanding of the vibrational structure is a phenomenon valid further than only at the small displacements around local minima and that the same modal character is retained even at higher-energy states in which interactions between modes can take place.

In Ref. 5, we further investigated the regular shapes of the excited vibrational modes and suggested a semi-automatic assignment procedure based on comparing the modal density shapes by means of overlap integrals. In our study of the water molecule,[5] about 200 vibrational states were assigned almost automatically, mostly without the need of visually checking the density plots. For water, a molecule with an Abelian molecular-symmetry (MS) group, C_{2v}(M),[21] and free of vibrational tunneling, we could also make use of a simple build-up principle that helped selecting the appropriate assignment out of several possibilities. For systems exhibiting tunneling splittings, the ordering of states is less "strict" (it is common that the tunneling splitting is large enough that the + and − states of the same origin enclose several other energy levels in between and there is also the possibility of exchanging the energy order of the + and − states), and one may not generally rely on such a simple automatic approach. In our study on water, we further realized that the full $\Gamma_1(q_i',q_i)$ matrix can actually reveal the true nodal structure of a particular mode by visible changes in sign. This is a stronger node indicator than just the variation of diagonal density and can be used complementarily for cases with barely recognizable nodes.

In the present study, we are focusing on the ammonia molecule, $^{14}NH_3$, which structurally is also a simple but dynamically considerably more challenging system than water, as ammonia exhibits tunneling and, at the same time, possesses two doubly degenerate vibrational modes. The obstacles hindering the assignment of the states arising from tunneling have been explained above. Next, we turn our attention to issues related to excitations that involve degenerate vibrational modes.

C. Excitations of a single twofold degenerate vibrational mode

Excitations of a twofold degenerate mode are traditionally described by a two-dimensional (2D) isotropic harmonic oscillator (TDIHO) model.[21] In that model, one transforms the two vibrational quantum numbers (v_1 v_2) (each of which corresponds to one of the two equivalent degenerate normal-coordinate components) into (v l), where v has the meaning of the total number of quanta in the 2D harmonic oscillator and l is the vibrational angular momentum quantum number describing the angular distribution of the 2D wave function. For a given number of quanta v, the wave function is (v + 1)-fold degenerate, with l values ranging v, v − 2, . . ., −v.

The TDIHO model perfectly fits a molecule such as acetylene, C_2H_2.[22] Nevertheless, considering the high multiplicity (v + 1) of the TDIHO associated angular momentum operator irreducible vector spaces, we can see that the group of the TDIHO model is necessarily superior to groups of other molecular Hamiltonians, which have mostly singly, doubly, or triply degenerate irreducible representations (irreps). Hence, the TDIHO-anticipated (v + 1)-fold degeneracy breaks for most molecular Hamiltonians and results in a decomposition of the *symmetric product* of the E representation with itself, denoted as $[E]^v$,[21] where the E irrep belongs to a group of a particular molecular Hamiltonian and not to the group of the TDIHO model. For example, in the C_{3v}(M) molecular-symmetry (MS) group,[21] the vibrational states having two quanta in the E vibrational mode decompose as

$$[E]^2 \equiv [E \otimes E] = A_1 \oplus E, \tag{8}$$

and analogously for the D_{3h}(M) group (see Table I). This immediately shows the breaking of the threefold degeneracy expected from

TABLE I. Decomposition of the symmetric product for a few powers of $[E]^v$ under C_{3v}(M) and $[E']^v$ and $[E'']^v$ under the D_{3h}(M) molecular-symmetry groups.

v	C_{3v}(M): $[E]^v$	D_{3h}(M): $[E']^v$	D_{3h}(M): $[E'']^v$
2	$A_1 \oplus E$	$A_1' \oplus E'$	$A_1' \oplus E'$
3	$A_1 \oplus A_2 \oplus E$	$A_1' \oplus A_2' \oplus E'$	$A_1'' \oplus A_2'' \oplus E''$
4	$A_1 \oplus 2\,E$	$A_1' \oplus 2\,E'$	$A_1' \oplus 2\,E'$
5	$A_1 \oplus A_2 \oplus 2\,E$	$A_1' \oplus A_2' \oplus 2\,E'$	$A_1'' \oplus A_2'' \oplus 2\,E''$
6	$2\,A_1 \oplus A_2 \oplus 2\,E$	$2\,A_1' \oplus A_2' \oplus 2\,E'$	$2\,A_1' \oplus A_2' \oplus 2\,E'$
7	$A_1 \oplus A_2 \oplus 3\,E$	$A_1' \oplus A_2' \oplus 3\,E'$	$A_1'' \oplus A_2'' \oplus 3\,E''$

the TDIHO theory into a single A_1 and a single E degenerate level. Therefore, we suggest that it is more appropriate to label single degenerate-mode excitations $(v\ \alpha)$ instead of $(v \pm l)$, where α denotes the appropriate irrep. Thus, for the aforementioned states, the labels would convert as

$$(2 \pm 2) \rightarrow (2\,E) \text{ and } (2\,0) \rightarrow (2\,A_1). \tag{9}$$

It is worth noting that this symmetric product decomposition treatment of degenerate systems is not confined to degenerate harmonic oscillator models but is valid for degenerate anharmonic oscillators as well.

Although the suggested $(v\ \alpha)$ labeling scheme may seem merely as a different notation to the $(v\ l)$ quantum numbers, it needs to be emphasized that

1. the information about the actual irrep (and degeneracy) is not directly available from the l quantum number in a general case, and
2. in Sec. II D, we explain that for systems with more than one degenerate mode (such as ammonia), labeling the individual modes by l does not generally make sense as it could lead to incorrect symmetry and it is also necessary to deal with the total irrep of all the excited degenerate modes, for which the knowledge of the α irreps is inevitable.

Because the decomposition of the symmetric product is not as straightforward as that of the ordinary direct product, in Table I, we recall the decomposition for a few powers of $[E]^v$ under C_{3v}(M) and $[E']^v$ and $[E'']^v$ under the D_{3h}(M) MS groups. Note that there are a number of publications detailing the use and treatment of symmetric (and antisymmetric) products in theoretical chemistry.[21,23–25]

D. Excitations of two twofold-degenerate vibrational modes

Care must be exercised when two degenerate modes are excited simultaneously. In the ammonia molecule, for example, there are two E' vibrational modes under the D_{3h}(M) group. Their simultaneous excitation by v_3 and v_4 quanta, respectively, leads to states decomposing as

$$[E']^{v_3} \otimes [E']^{v_4} = \sum_i^{\text{irreps}} c_i\,\Gamma_i, \tag{10}$$

TABLE II. Decomposition of simultaneous excitation of the two degenerate vibrational modes of ammonia for both C_{3v}(M) and D_{3h}(M) symmetry models.

v_3	v_4	C_{3v}(M): $[E]^{v_3} \otimes [E]^{v_4}$	D_{3h}(M): $[E']^{v_3} \otimes [E']^{v_4}$
1	1	$A_1 \oplus A_2 \oplus E$	$A_1' \oplus A_2' \oplus E'$
1	2	$A_1 \oplus A_2 \oplus 2\,E$	$A_1' \oplus A_2' \oplus 2\,E'$
1	3	$A_1 \oplus A_2 \oplus 3\,E$	$A_1' \oplus A_2' \oplus 3\,E'$
1	4	$2\,A_1 \oplus 2\,A_2 \oplus 3\,E$	$2\,A_1' \oplus 2\,A_2' \oplus 3\,E'$
1	5	$2\,A_1 \oplus 2\,A_2 \oplus 4\,E$	$2\,A_1' \oplus 2\,A_2' \oplus 4\,E'$
2	2	$2\,A_1 \oplus A_2 \oplus 3\,E$	$2\,A_1' \oplus A_2' \oplus 3\,E'$
2	3	$2\,A_1 \oplus 2\,A_2 \oplus 4\,E$	$2\,A_1' \oplus 2\,A_2' \oplus 4\,E'$
2	4	$3\,A_1 \oplus 2\,A_2 \oplus 5\,E$	$3\,A_1' \oplus 2\,A_2' \oplus 5\,E'$
3	3	$3\,A_1 \oplus 3\,A_2 \oplus 5\,E$	$3\,A_1' \oplus 3\,A_2' \oplus 5\,E'$

where Γ_i stands for the ith irreducible representation of the D_{3h}(M) group. For other systems possessing multiple degenerate dofs under different symmetry groups and different excited combinations of degenerate irreps, the generalization of Eq. (10) is straightforward. For the combination of two (or more) degenerate modes, the resulting multimode excitation has to be labeled both by the resulting irrep and by all the excitation quantum numbers of individual contributing degenerate modes such as $(v_3\ v_4\ \alpha)$, where α stands for the particular irrep. In Table II, we provide decompositions of several excited combinations of the two degenerate modes of ammonia in both the C_{3v}(M)- and the D_{3h}(M)-symmetry models. An excitation labeled (1 2 1E') would mean a state formed by $v_3 = 1$ quantum in one E' degenerate mode and $v_4 = 2$ quanta in the other E' degenerate mode, making together the E' irrep. Since there are two E' irreps coming from the $v_3 = 1$ and $v_4 = 2$ excitations, we need to give the E' irrep an additional index, 1 (see Table II).

In principle, one could label the individual modes with their symmetric-product labels $(v\ \alpha)$, but it remains inevitable to provide the resulting irrep label. Otherwise, the labeling would not be unique. This is apparent from Table III for the $v_3 = 1$ and $v_4 = 2$ states, where we compare our suggested labeling scheme, which is unique, with the combination of individual mode labels, which is ambiguous. However, one cannot use a particular component of the degenerate irrep for labeling the individual modes as it would not generally result in a pure irrep of the given symmetry group. That would be the same mistake as constructing a two-electron singlet spin state as a simple product of the α and β spin functions and ignoring the proper Clebsch–Gordan expansion[24] that leads

TABLE III. An example showing the uniqueness of the newly suggested labeling scheme for excited combinations of degenerate modes, in contrast to the ambiguous use of individual degenerate mode labels for the $v_3 = 1$ and $v_4 = 2$ excitation numbers within the C_{3v}(M) symmetry model.

$(v_3\ v_4\ \alpha)$	$(v_3\ \alpha_3)\ (v_4\ \alpha_4)$
(1 2 A_1)	(1 E) (2 E)
(1 2 A_2)	(1 E) (2 E)
(1 2 1E)	(1 E) (2 A_1)
(1 2 2E)	(1 E) (2 E)

to the well-known $\frac{1}{\sqrt{2}}(\alpha\beta - \beta\alpha)$ combination. The appropriate Clebsch–Gordan expansion of the resulting vibrational state in the direct-product space of v_3 and v_4 modes generally reads

$$|v_3\, v_4\, \Gamma_i\, j\rangle = \sum_{\alpha_k\beta_k} |[E']^{v_3}\, \alpha_k\rangle\, |[E']^{v_4}\, \beta_k\rangle\; C^{ij}_{\alpha_k\beta_k}(v_3, v_4), \tag{11}$$

where $|v_3\ v_4\ \Gamma_i\ j\rangle$ is the jth [$j = 1 \ldots c_i$; see Eq. (10)] state of Γ_i irrep formed by the v_3-quanta-excited v_3 mode and the v_4-quanta-excited v_4 mode [see Eq. (10)], $|[E']^{v_3}\, \alpha_k\rangle$ is the kth component of the αth irrep produced from the v_3-fold symmetric product of the v_3th E' irrep with itself (note that for one-dimensional α irrep, the index k is just 1), $|[E']^{v_4}\, \beta_k\rangle$ is analogous, and $C^{ij}_{\alpha_k\beta_k}(v_3, v_4)$ is the corresponding Clebsch–Gordan coefficient.

In contrast to the traditional use of vibrational angular momentum quantum number pairs, $(v\ l)$, the labeling scheme suggested above directly provides the symmetry and the degeneracy of the resulting states. Moreover, for reasons explained in the previous paragraph and directed by Eq. (11), the labeling with a simple product of $(v_3\ l_3)$ and $(v_4\ l_4)$ modal quantum numbers, which is common for the vibrational assignment of systems such as ammonia, cannot generally lead to the proper state symmetry. Nevertheless, such a labeling still remains unique, and it is sufficient in that sense.

III. COMPUTATIONAL DETAILS

A. Internal coordinates and embedding

The vibrational motion of the ammonia molecule is parameterized, as shown in Figs. 1 and 2. Before shifting the center of nuclear mass into the origin of the coordinate system, the coordinates of the individual atoms read as

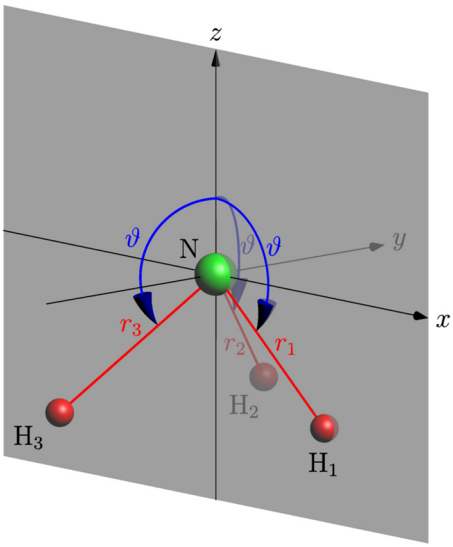

FIG. 1. Vibrational parameters r_1, r_2, r_3, and ϑ of the ammonia molecule with the xz plane shaded.

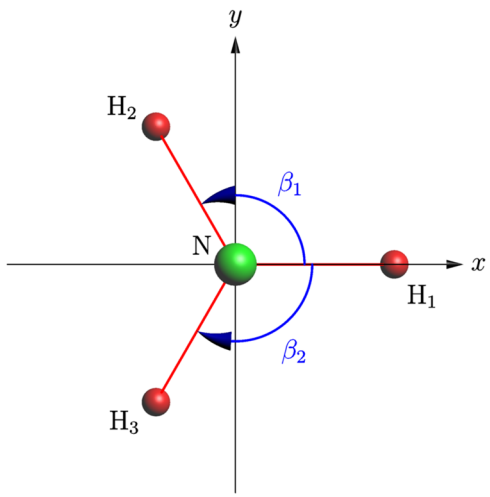

FIG. 2. The β_1 and β_2 vibrational parameters of ammonia shown in the xy projection.

	x	y	z
N	0	0	0
H_1	$r_1 \sin\vartheta$	0	$r_1 \cos\vartheta$.
H_2	$r_2 \sin\vartheta \cos\beta_1$	$r_2 \sin\vartheta \sin\beta_1$	$r_2 \cos\vartheta$
H_3	$r_3 \sin\vartheta \cos\beta_2$	$-r_3 \sin\vartheta \sin\beta_2$	$r_3 \cos\vartheta$

(12)

The actual internal coordinates are symmetry adapted in the radial parameters with respect to permutations of the hydrogen atoms, which gives $q_1 = r_1 + r_2 + r_3$, $q_2 = 2r_1 - r_2 - r_3$, $q_3 = r_2 - r_3$, $q_4 = \vartheta$, $q_5 = \beta_1$, and $q_6 = \beta_2$. Such an internal-coordinate system has been chosen to mimic the harmonic oscillator-like vibrational modes. The mapping between the internal coordinates and the associated modes is given in Table IV.

B. Variational computations

Variational computation of the vibrational states of $^{14}NH_3$ has been performed using our in-house nuclear-motion code GENIUSH,[26,27] where the abbreviation stands for a general (GE), numerical (N) rovibrational code employing curvilinear internal (I) coordinates and user-specified (US) Hamiltonian (H). Altogether, 600 vibrational states of $^{14}NH_3$ have been computed on a direct-product grid utilizing the parameters shown in Table V. The individual coordinates are represented by Hermite- or

TABLE IV. Vibrational modes with the associated internal coordinates and symmetries.

Mode	Coords.	Corresponding normal mode	Symmetry
ν_1	q_1	Symmetric stretch	A_1
ν_2	q_4	Umbrella motion	A_1
ν_3	q_2, q_3	Antisymmetric stretch	E
ν_4	q_5, q_6	Antisymmetric bend	E

TABLE V. Parameters of individual internal coordinates in the computational direct-product grid. The radial values are in bohr, and the angles are in degrees.

Coord.	Min	Max	Type	Number of DVR points	Number of PO-DVR points	PO-DVR Ref. Conf.
q_1	4.40	7.55	Hermite	300	10	5.6373
q_2	−1.80	2.10	Hermite	300	10	0.0000
q_3	−1.20	1.20	Hermite	300	10	0.0000
q_4	40	140	Legendre	101	48	90.0
q_5	70	179	Hermite	23	...	120.0
q_6	70	179	Hermite	23	...	120.0

Legendre-type discrete-variable-representation (DVR)[28,29] grid points, four of them further reduced by the potential-optimized (PO-DVR) procedure with a planar reference molecular configuration. The large-scale eigenvalue problem is solved by the iterative Lanczos algorithm.[30]

The spectroscopic potential NH3-Y2010[31] of Yurchenko and co-workers has been employed during the nuclear-motion computations. The masses of the hydrogen and nitrogen nuclei were set to $m_{\mathrm{H}} = 1.007\,825$ u and $m_{\mathrm{N}} = 14.003\,074$ u, respectively.

IV. RESULTS, ANALYSIS, AND DISCUSSION

During this study, altogether, 600 vibrational states of ammonia have been computed and the majority of them assigned. A concise comparison of our results to the recently published CoYuTe[6] line list is reported in the supplementary material. A selection of states relevant for this discussion is shown in Table VI. The actual comparison is made only after the first two subsections, which discuss the density structure of the computed excited states with the associated

TABLE VI. Comparison of vibrational states from the CoYuTe[6] list with the results of this work. The energy level ordering is that given by the CoYuTe list. Indices of the states provided by the CoYuTe list and indices of the computed eigenstates of this study are also shown. The excitation energies are given as wavenumbers (cm^{-1}) with respect to the vibrational ground state. The zero-point vibrational energy (ZPVE) computed in this study is 7430.28 cm^{-1}. The labels are [n_1, n_2 p, n_3 n_4 α], and the CoYuTe labels also include the (l_3 l_4) quantum numbers (see the text for details). The molecular-symmetry (MS) group used is D_{3h}(M). The two components of the degenerate E' and E'' states of this work are distinguished by + and − subscripts.

			CoYuTe		This work	
Level	Index	E	Label	Index	E	Label
1	1	0.00	[0, 0+, 0 0 A_1'(0 0)]	1	0.00	[0, 0+, 0 0 A_1']
2	7779	0.79	[0, 0−, 0 0 A_2'' (0 0)]	2	0.79	[0, 0−, 0 0 A_2'']
3	2	932.43	[0, 1+, 0 0 A_1'(0 0)]	3	932.48	[0, 1+, 0 0 A_1']
4	7780	968.12	[0, 1−, 0 0 A_2'' (0 0)]	4	968.13	[0, 1−, 0 0 A_2'']
5	3	1597.48	[0, 2+, 0 0 A_1'(0 0)]	5	1597.50	[0, 2+, 0 0 A_1']
6	3249	1626.27	[0, 0+, 0 1 E' (0 1)]	6	1626.20	[0, 0+, 0 1 E_+']
				7	1626.20	[0, 0+, 0 1 E_-']
7	9447	1627.37	[0, 0−, 0 1 E'' (0 1)]	8	1627.29	[0, 0−, 0 1 E_+'']
				9	1627.29	[0, 0−, 0 1 E_-'']
8	7781	1882.18	[0, 2−, 0 0 A_2'' (0 0)]	10	1882.11	[0, 2−, 0 0 A_2'']
10	3250	2540.52	[0, 1+, 0 1 E' (0 1)]	12	2540.40	[0, 1+, 0 1 E_+']
				13	2540.40	[0, 1+, 0 1 E_-']
14	5	3215.95	[0, 0+, 0 2 A_1'(0 0)]	19	3215.75	[0, 0+, 0 2 A_1']
16	3252	3240.16	[0, 0+, 0 2 E' (0 2)]	21	3240.13	[0, 0+, 0 2 E_+']
				22	3240.14	[0, 0+, 0 2 E_-']
20	3253	3443.63	[0, 0+, 1 0 E' (1 0)]	27	3443.45	[0, 0+, 1 0 E_+']
				28	3443.54	[0, 0+, 1 0 E_-']
38	3258	4799.22	[0, 0+, 0 3 E' (0 1)]	55	4799.12	[0, 0+, 0 3 E_+']
				56	4799.12	[0, 0+, 0 3 E_-']
40	1825	4840.89	[0, 0+, 0 3 A_2'(0 3)]	60	4842.09	[0, 0+, 0 3 A_2']

TABLE VI. *(Continued.)*

			CoYuTe		This work	
Level	Index	E	Label	Index	E	Label
41	12	4841.55	[0, 0+, 0 3 A_1'(0 3)]	59	4841.33	[0, 0+, 0 3 A_1']
42	6482	4842.96	[0, 0—, 0 3 A_1'' (0 3)]	62	4844.01	[0, 0—, 0 3 A_1'']
43	7788	4843.36	[0, 0—, 0 3 A_2'' (0 3)]	61	4842.48	[0, 0—, 0 3 A_2'']
47	1826	5052.02	[0, 0+, 1 1 A_2'(1 1)]	68	5051.17	[0, 0+, 1 1 A_2']
48	3260	5052.60	[0, 0+, 1 1 E' (1 1)]	70	5052.36	[0, 0+, 1 1 E_+']
				71	5052.37	[0, 0+, 1 1 E_-']
52	14	5067.78	[0, 0+, 1 1 A_1'(1 1)]	74	5069.62	[0, 0+, 1 1 A_1']
85	20	6348.84	[0, 2+, 0 3 A_1'(0 3)]	124	6341.36	[0, 2+, 0 3 A_1']
88	21	6356.07	[0, 2+, 0 3 A_1'(0 3)]	128	6354.33	[0, 0+, 0 4 A_1']
Note: CoYuTe misassignment; see level 85						
101	3274	6608.82	[1, 0+, 1 0 E' (1 0)]	148	6607.21	[1, 0+, 1 0 E_-']
				149	6607.55	[1, 0+, 1 0 E_+']
103	24	6650.82	[0, 0+, 1 2 A_1'(1 2)]	152	6647.32	[0, 0+, 1 2 A_1']
104	1830	6650.91	[0, 0+, 1 2 A_2'(1 2)]	154	6650.66	[0, 0+, 1 2 A_2']
108	3275	6666.07	[0, 0+, 1 2 E' (1 2)]	156	6666.82	[0, 0+, 1 2 1E_+']
				157	6666.88	[0, 0+, 1 2 1E_-']
109	3276	6677.43	[1, 0+, 1 0 E' (1 0)]	162	6676.34	[0, 0+, 1 2 2E_+']
				163	6676.60	[0, 0+, 1 2 2E_-']
Note: CoYuTe misassignment; see level 101						
173	37	7860.33	[0, 2+, 0 4 A_1'(0 0)]	252	7834.07	[0, 2+, 0 4 A_1']
Note: Noticeably far lower energy in this work; see also level 175						
175	3292	7875.62	[0, 2+, 0 4 E' (0 2)]	255	7852.87	[0, 2+, 0 4 1E_+']
				256	7853.15	[0, 2+, 0 4 1E_-']
Note: Noticeably far lower energy in this work; see also level 173						
195	1836	8135.74	[1, 0+, 1 1 A_2'(1 1)]	289	8131.49	[1, 0+, 0 3 A_2']
Note: CoYuTe misassignment; see level 222						
200	1837	8174.12	[0, 0+, 1 3 A_2'(1 1)]	300	8175.03	[0, 0+, 1 3 A_2']
215	9496	8261.26	[0, 2—, 0 4 E'' (0 2)]	314	8246.27	[0, 2—, 0 4 1E_+'']
				315	8246.56	[0, 2—, 0 4 1E_-'']
Note: Noticeably far lower energy in this work						
222	1839	8285.96	[0, 0+, 1 3 A_2'(1 1)]	333	8283.76	[1, 0+, 1 1 A_2']
Note: CoYuTe misassignment; see level 200						
234	3309	8423.94	[1, 4+, 0 1 E' (0 1)]	347	8418.16	[1, 4+, 0 1 E_-']
				348	8418.23	[1, 4+, 0 1 E_+']
271	9510	8937.31	[1, 4—, 0 1 E'' (0 1)]	413	9013.63	[1, 4—, 0 1 E_-'']
				415	9013.74	[1, 4—, 0 1 E_+'']
Note: Noticeably far higher energy in this work						
328	7835	9436.75	[1, 0—, 0 4 A_2'' (0 0)]	487	9415.74	[0, 0—, 0 6 1A_2'']
Note: CoYuTe misassignment						

peculiarities of the ammonia molecule (Sec. IV A) and the actual assignment process (Sec. IV B).

In this study, we use the following notation for labeling the ammonia vibrational states: [n_1, n_2 p, n_3 n_4 α], where n_1, n_2, n_3, and n_4 are the number of quanta in the respective vibrational modes (see Table IV), the parity p is either "+" or "−," reflecting the inversion symmetry of the molecule, and it is associated with the umbrella-motion-like coordinate q_2, while α is the resulting irrep [in

the D_{3h}(M) group] of the (ν_3 ν_4) pair of degenerate modes. Labels in the CoYuTe list are in addition provided with the vibrational angular momentum quantum numbers l_3 and l_4, which we place in parentheses as the last descriptor of the full label.

At this point, we need to clarify the distinction between the terms *state* and *energy level*, terms we extensively use in this section. In this context, the meaning of these terms cannot be freely interchanged. By an energy level, we mean a particular eigenvalue of the Hamiltonian operator, no matter whether it is degenerate or not. However, the states are attributed to particular eigenvectors of the Hamiltonian, that is, one degenerate level corresponds to several states. Since the GENIUSH code that we employ in the computation of the Hamiltonian eigenstates cannot make full use of symmetry, the resulting eigenstates do not have perfectly degenerate numerical values for the eigenenergies. Thus, we provide two energy values, together with two eigenstates, for a single degenerate level. The CoYuTe list, by contrast, provides only one value for each energy level.

A. Structure of the vibrational states of ammonia

It may seem straightforward to represent the individual vibrational modes of $^{14}NH_3$ by the following density matrices: ν_1 as $\Gamma_1(q_1', q_1)$, ν_2 as $\Gamma_1(q_4', q_4)$, ν_3 as $\Gamma_2^{\mathrm{D}}(q_2, q_3)$, and ν_4 as $\Gamma_2^{\mathrm{D}}(q_5, q_6)$. The first ten states, indeed, are concisely described this way, as shown in Fig. 3, where states are in rows and the columns correspond to the various density matrices. For the ground state, state No. 1, the density is concentrated in a simple area around the equilibrium geometry. There are two equivalent energy minima on the PES of $^{14}NH_3$ related by the inversion symmetry operation and accessed mutually by tunneling via the umbrella-motion-like coordinate q_4. This is why both minima are populated in the $\Gamma_1(q_4', q_4)$ plot; see the two red areas on the bottom-left to upper-right diagonal. The other two populated areas (on the upper-left to bottom-right diagonal), representing the cross-terms of the RDM [Eq. (3)], correspond to a product of the wave function in one minimum with the wave function in the other minimum. Comparing plots of the first two states, which differ only in the sign of these two cross-term areas, we can deduce that the ground state has the same wave-function sign in both minima and has thus "+" symmetry with respect to the inversion operation. State No. 2 changes the wave-function sign between the two minima, and it is thus assigned with the "−" symmetry label. In states Nos. 3 and 4, we can see a single wave-function node in each of the two minima, suggesting that the ν_2 mode is singly excited. From the symmetry of the sign distribution in the $\Gamma_1(q_4', q_4)$ density plot, we can easily deduce "+" symmetry for state No. 3 and "−" symmetry for state Nos. 4. State 5 is doubly excited in ν_2 and has "+" symmetry, and its "−" partner is state No. 10. States Nos. 6 and 7 are degenerate, singly excited in mode ν_4, with "+" symmetry. Their complementary "−" states are Nos. 8 and 9, respectively. One should note that the $\Gamma_2^{\mathrm{D}}(q_5, q_6)$ densities might more naturally be functions of the $q_5 + q_6$ and $q_5 - q_6$ coordinate combinations.

Figure 4 shows another selection of relatively simple states worth commenting on for an improved understanding of higher-energy states. State No. 12 is a combination of a single ν_2 mode excitation with "+" symmetry and a single ν_4 mode excitation (one of its degenerate components), as can be deduced by comparing the

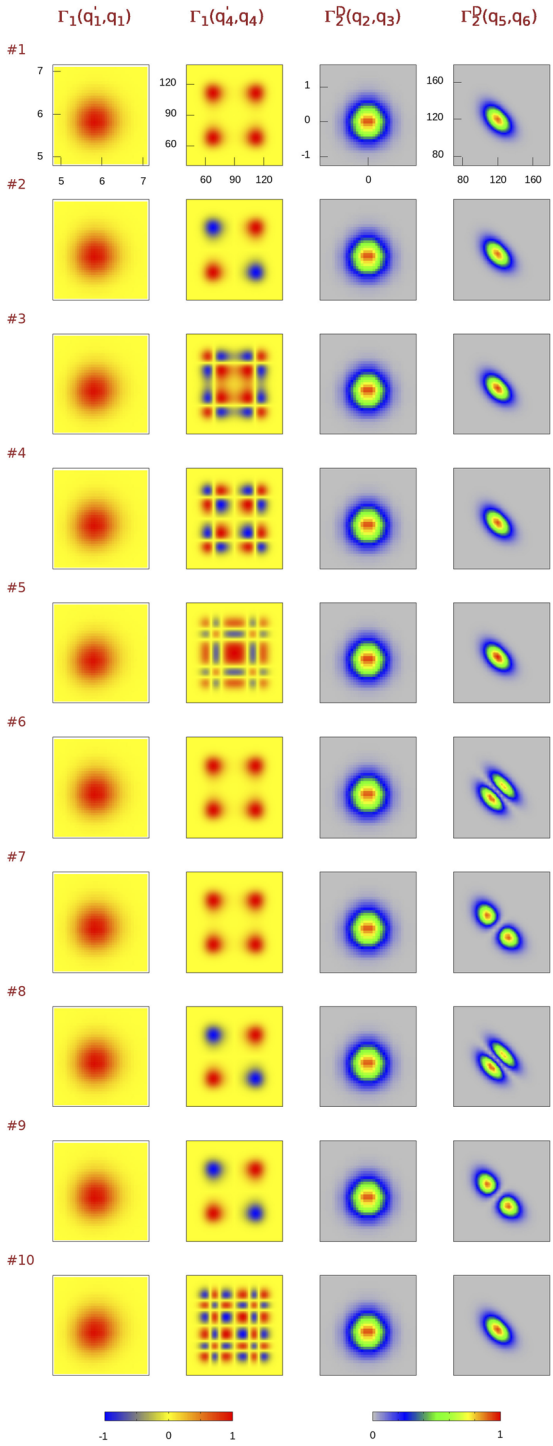

FIG. 3. First ten vibrational states of ammonia (rows) depicted for each of its vibrational modes (columns) by an appropriate two-dimensional reduced-density matrix. First of the two dimensions corresponds to the vertical axis of the plots, while the other dimension corresponds to the horizontal axis. The stretching coordinates q_{1-3} use atomic units, and the bending coordinates q_{4-6} use degrees. Scale of the densities is shown by the color boxes underneath.

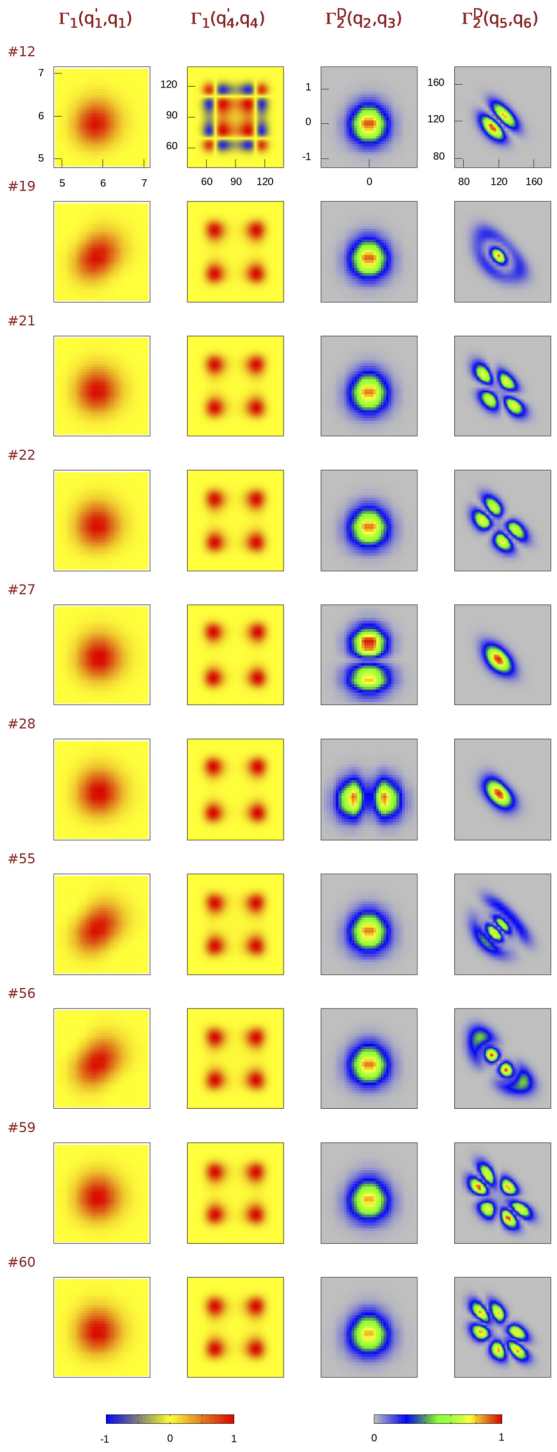

FIG. 4. Selected vibrational states of ammonia (rows) depicted for each of its vibrational modes (columns) by an appropriate two-dimensional reduced-density matrix. First of the two dimensions corresponds to the vertical axis of the plots, while the other dimension corresponds to the horizontal axis. The stretching coordinates q_{1-3} use atomic units, and the bending coordinates q_{4-6} use degrees. Scale of the densities is shown by the color boxes underneath.

densities of states Nos. 3 and 6. It turns out that for the vast majority of cases, the excitation structure of the states can be easily deduced in the same way by comparing shapes of the individual mode RDMs. States Nos. 19, 21, and 22 correspond to the doubly excited ν_4 mode. The threefold degeneracy of the TDIHO model is split under the D_{3h}(M) MS group into the A_1' irrep of state No. 19 and the doubly degenerate E' irrep of states Nos. 21 and 22 (see Table I). States Nos. 27 and 28 are degenerate singly excited ν_3 modes, and one can note that each of the E' irrep components is already well described by the single internal coordinate, in contrast to the excited ν_4 mode commented above. The four states Nos. 55, 56, 59, and 60 represent the triply excited ν_4 mode, which is split into the degenerate E' (Nos. 55, 56) and separate A_1' and A_2' irreps (Nos. 59 and 60, respectively).

In Fig. 5, another type of state is shown, in which both E' degenerate modes are excited simultaneously. One can immediately note that the density shapes of the two E' modes (ν_3 and ν_4) are not simple combinations of densities of only individually excited ν_3 or ν_4 modes. The assignment is thus more complicated than what has just been described for states with only one of the two degenerate modes excited. States Nos. 68, 70, 71, and 74 have both the ν_3 and ν_4 modes singly excited, which leads to state symmetries,

$$E' \otimes E' = A_1' \oplus A_2' \oplus E'. \tag{13}$$

Thanks to the observed (computationally obtained) degeneracy of the states, states Nos. 70 and 71 can be assigned with the E' label. Otherwise, the states are hardly distinguishable or assignable just by comparing the two-dimensional densities, which all look almost the same in a given mode. Since all the RDM plots look very similar and they do not resemble any of the E' RDM shapes of the individual singly excited ν_3 or ν_4 mode patterns (i.e., states Nos. 6, 7, 27, and 28) so that we could assign each of the two modes by one component of its E' degenerate pair, we can conclude, in accordance with Sec. II D, that every time both E' modes are excited simultaneously, it is necessary to treat both E' modes as a single two-mode-unit with a complex label specifying the distribution of the quanta between the two modes and also the resulting irrep, which needs to be known from the computation or examined explicitly. Thus, the complex two-mode-unit label of all these states has one quantum in mode ν_3, one quantum in mode ν_4, and the resulting symmetry of the two-mode-unit is A_1' or A_2' or E'. A shorthand notation is, for example, $(1\,1\,A_1')$.

The other six states in Fig. 5 correspond to singly excited ν_3 and doubly excited ν_4 modes, which decompose as

$$E' \otimes [E']^2 = E' \otimes (A_1' \oplus E') = A_1' \oplus A_2' \oplus 2E'. \tag{14}$$

Labeling the non-degenerate states Nos. 152 and 154 by mere visual inspection of the depicted densities is not productive, and the explicit knowledge of their irreps is necessary. Looking at the ν_3 density in the degenerate states (Nos. 156, 157, 162, 163), one cannot fail to note a single excitation pattern similar to the one in states Nos. 27 and 28. The ν_4 mode in these four states exhibits a clear degenerate doubly excited density pattern, which, however, is very different from the one in states Nos. 21 and 22. This reaffirms the above-mentioned observation that excitations of a single degenerate

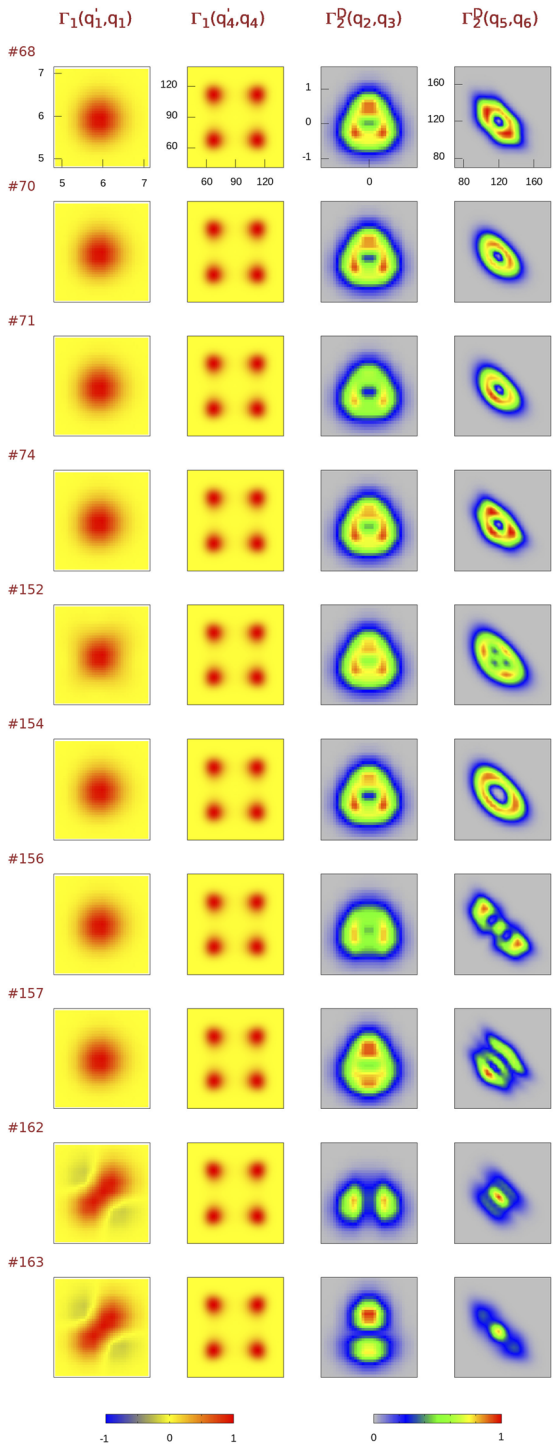

FIG. 5. Selected vibrational states of ammonia (rows) depicted for each of its vibrational modes (columns) by an appropriate two-dimensional reduced-density matrix. First of the two dimensions corresponds to the vertical axis of the plots, while the other dimension corresponds to the horizontal axis. The stretching coordinates q_{1-3} use atomic units, and the bending coordinates q_{4-6} use degrees. Scale of the densities is shown by the color boxes underneath.

mode need a different treatment than combined excitation of two (or generally more) degenerate modes.

To successfully distinguish between the highly similar and rather featureless density representations of states possessing several excited degenerate modes, it is inevitable to resolve the two-dimensional quantities in yet another dimension. Since the only way how to resolve a mode's RDM structure more deeply means the involvement of another coordinate that is intrinsic to a different mode, it actually means that the modes are *a priori* coupled. This, again, confirms the necessity of treating all degenerate modes together and not individually. The new dimension has to be taken from one of the two coordinates describing the other degenerate mode so that the three-dimensional quantity serves to characterize all the coupled modes. How to distinguish the degenerate states Nos. 70 and 71, by resolving the degenerate ν_3 and ν_4 modes in three-dimensional densities $\Gamma_3^{\mathrm{D}}(q_5, q_2, q_3)$ and $\Gamma_3^{\mathrm{D}}(q_2, q_5, q_6)$, is shown in Figs. 6 and 7. Apart from resolving the circular 2D density shapes, which we see in Fig. 5, into more informative 3D structures, one can see why these states are degenerate as their densities symmetrically differ only in their orientation. Even more remarkable is that we can see that the modal densities are composed of both E' irrep components, that is, the combination of the ν_3 densities of states Nos. 27 and 28 and ν_4 densities of states Nos. 6 and 7. This observation actually confirms the theoretically expected behavior of a pair of excited degenerate modes (see Sec. II D) that cannot be expressed as a single product of respective degenerate irrep basis components but is a combination analogous to the Clebsch–Gordan expansion. Similarly, in Figs. 8 and 9, we resolve states Nos. 152 and 154, respectively, which have one quantum in ν_3 and two quanta in the ν_4 modes. By looking at the $\Gamma_3^{\mathrm{D}}(q_2, q_5, q_6)$ density, which corresponds to the ν_4 mode (Fig. 7), and going down the q_2 coordinate, one can clearly note a transition between density structures recognized in the degenerate states Nos. 21 and 22. Nevertheless, the states Nos. 152 and 154 are not degenerate. As the last example, we resolve the degenerate states Nos. 156 and 157 in Figs. 10 and 11, respectively. One can see there that the 3D density structure is more complex than what might have been deduced from the relatively simple-looking 2D plots of Fig. 5.

In summary, to understand the multidimensional structure of vibrational wave functions, one has to start with a wise choice of the coordinate system that mimics well the modes of vibrations. Apart from the symmetry of a particular state's wave function, which is given by the computation or examined explicitly via projection techniques, the structure of the individual modes can be inspected by means of appropriate reduced-density matrices. Each mode's excitation leads to a characteristic RDM pattern that can either be assessed visually or effectively compared between other states by computing RDM overlaps and quickly recognized by pattern matching. This technique is readily applicable to non-degenerate vibrational modes. For a single degenerate mode that is excited, one has to take into account the proper symmetry of the states into which the given excited mode decomposes, as discussed in Sec. II C. In systems with more than one degenerate mode, such as ammonia, one has to treat all the degenerate modes with a single comprehensive label describing both the distribution of quanta among the degenerate modes and also the resulting symmetry of all those coupled degenerate modes, as described in Sec. II D. In order to distinguish the RDMs of the degenerate modes by pattern matching and to correctly assign

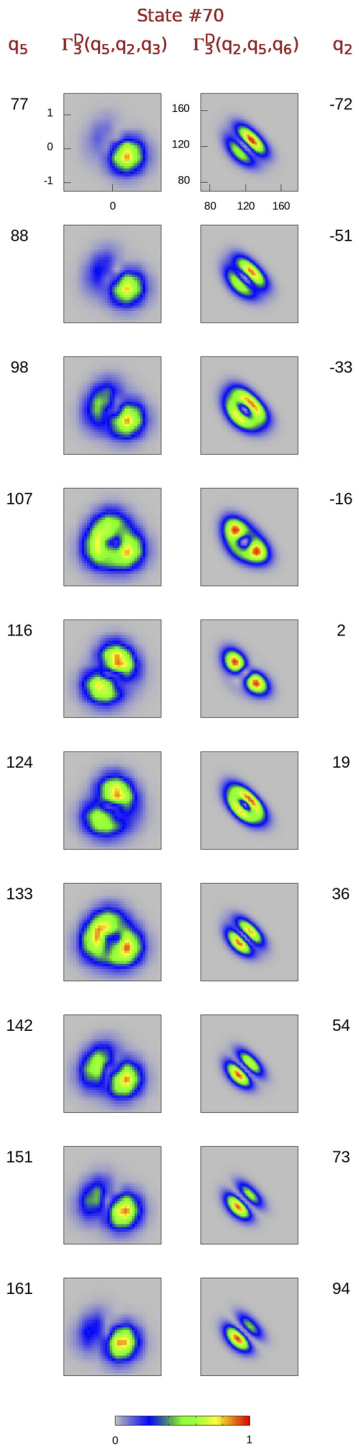

FIG. 6. Resolution of the degenerate vibrational modes by a third dimension of an appropriate reduced-density matrix for the selected state. Each row depicts two-dimensional submatrices of the three-dimensional RDMs with the first dimension fixed at a given coordinate value. The stretching coordinates q_{2-3} use atomic units, and the bending coordinates q_{5-6} use degrees. Scale of the densities is shown by the color box underneath.

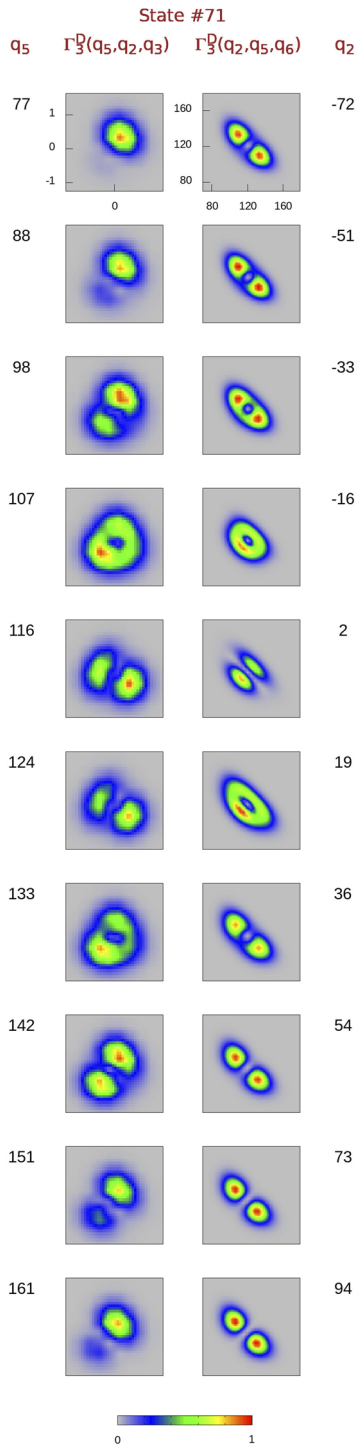

FIG. 7. Resolution of the degenerate vibrational modes by a third dimension of an appropriate reduced-density matrix for the selected state. Each row depicts two-dimensional submatrices of the three-dimensional RDMs with the first dimension fixed at a given coordinate value. The stretching coordinates q_{2-3} use atomic units, and the bending coordinates q_{5-6} use degrees. Scale of the densities is shown by the color box underneath.

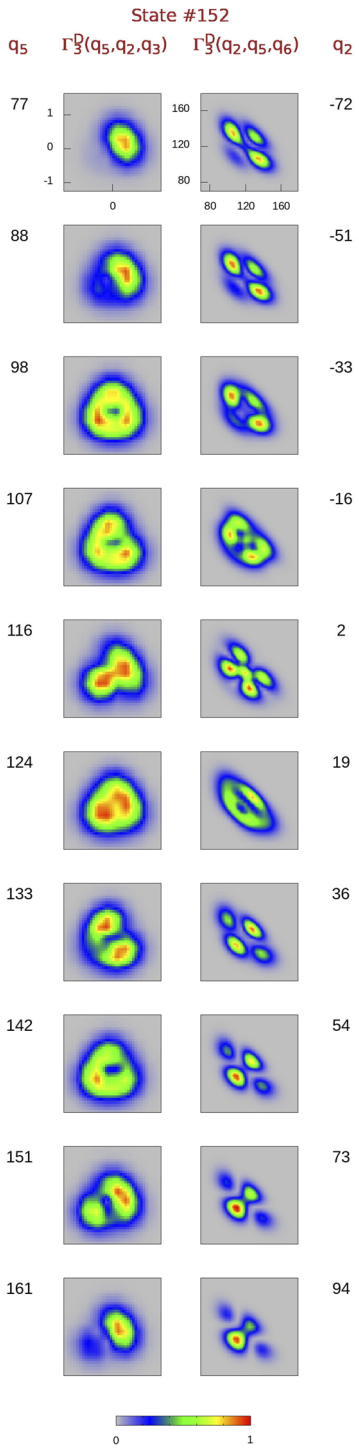

FIG. 8. Resolution of the degenerate vibrational modes by a third dimension of an appropriate reduced-density matrix for the selected state. Each row depicts two-dimensional submatrices of the three-dimensional RDMs with the first dimension fixed at a given coordinate value. The stretching coordinates q_{2-3} use atomic units, and the bending coordinates q_{5-6} use degrees. Scale of the densities is shown by the color box underneath.

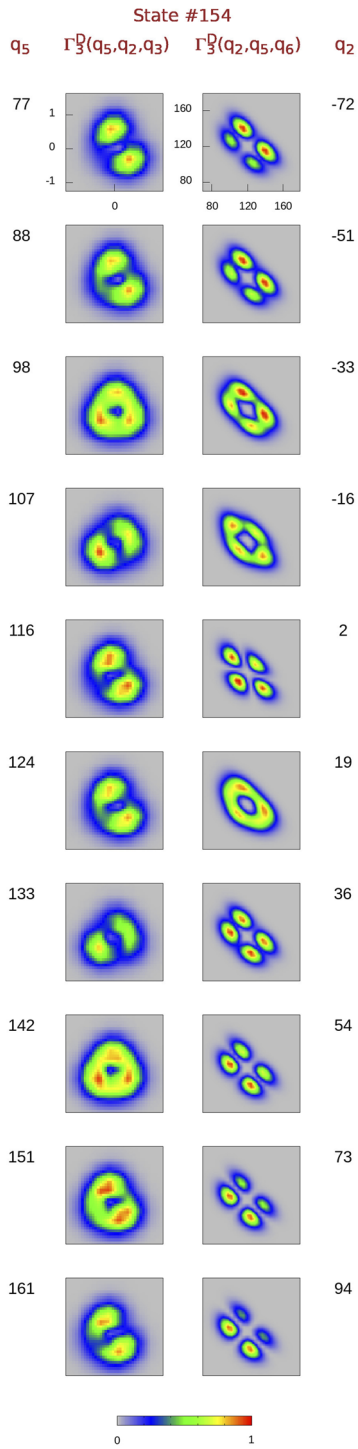

FIG. 9. Resolution of the degenerate vibrational modes by a third dimension of an appropriate reduced-density matrix for the selected state. Each row depicts two-dimensional submatrices of the three-dimensional RDMs with the first dimension fixed at a given coordinate value. The stretching coordinates q_{2-3} use atomic units, and the bending coordinates q_{5-6} use degrees. Scale of the densities is shown by the color box underneath.

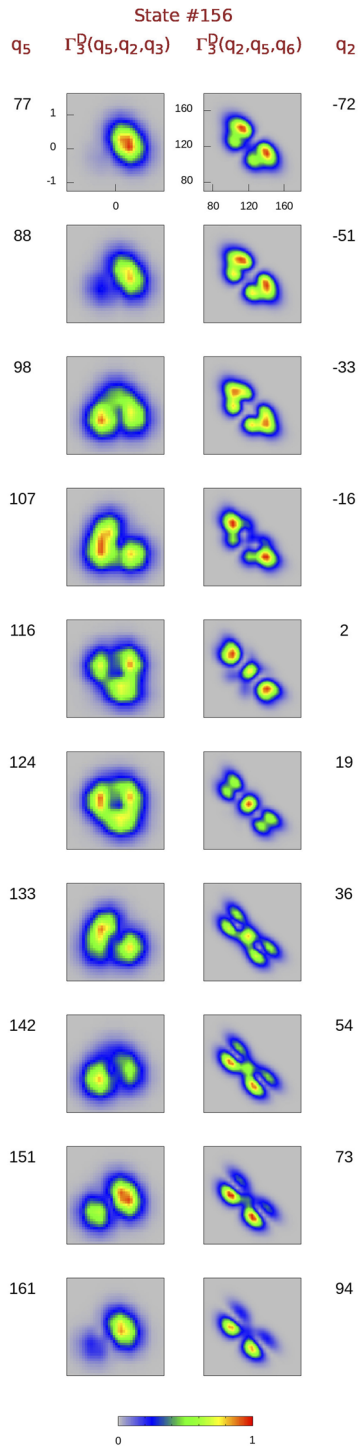

FIG. 10. Resolution of the degenerate vibrational modes by a third dimension of an appropriate reduced-density matrix for the selected state. Each row depicts two-dimensional submatrices of the three-dimensional RDMs with the first dimension fixed at a given coordinate value. The stretching coordinates q_{2-3} use atomic units, and the bending coordinates q_{5-6} use degrees. Scale of the densities is shown by the color box underneath.

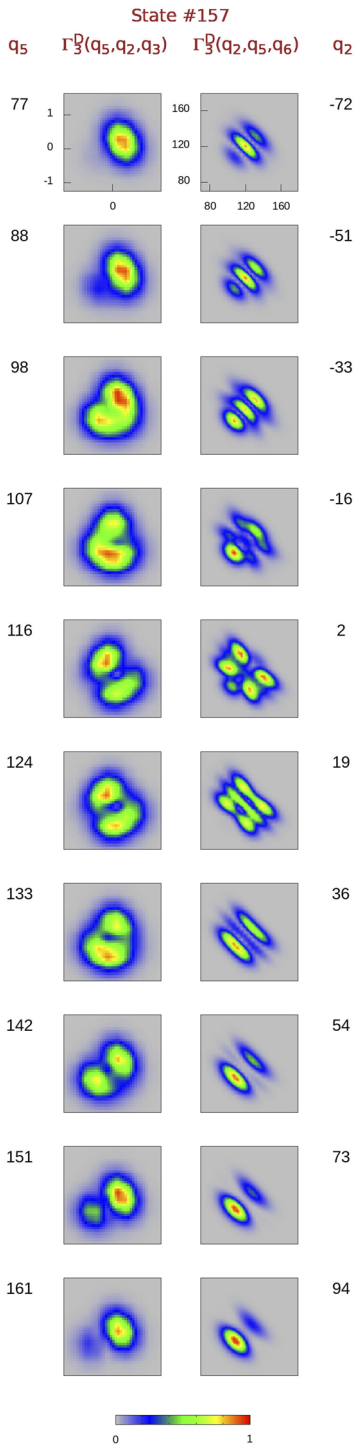

FIG. 11. Resolution of the degenerate vibrational modes by a third dimension of an appropriate reduced-density matrix for the selected state. Each row depicts two-dimensional submatrices of the three-dimensional RDMs with the first dimension fixed at a given coordinate value. The stretching coordinates q_{2-3} use atomic units, and the bending coordinates q_{5-6} use degrees. Scale of the densities is shown by the color box underneath.

the excited states, each individual (degenerate) mode RDM has to be additionally a function of other coordinates that are specific to all the other degenerate modes.

B. The actual assignment process

There are three basic assumptions behind RDM-based vibrational assignments. First, the chosen coordinate system must mimic the nuclear motion of real vibrational modes. Second, the multimode-excited wave-function density resembles densities of individually excited modes. Third, the densities of individual mode excitations are the characteristic and remain almost constant (i.e., recognizable) throughout a large number of excited states. We note here that the first assumption is mainly a practical prerequisite so that one can visually associate a particular mode excitation to an appropriate quantum number. In other words, one can use an arbitrary coordinate system, provided that there is a way of associating particular densities with appropriate quantum numbers, which is easily accomplished if coordinates mimicking normal modes are used, for instance. Once a density pattern is known for a particular mode excitation, there is actually no more need for the visual assessment of the density shapes as all is done automatically by pattern matching, even for oddly looking densities. To work with the actual densities and assign the states based on them with appropriate labels, we used a set of convenient auxiliary codes that made the assignment process relatively straightforward and semi-automatic. The algorithm has four major components.

First, each individual state was labeled with symmetry, by computing wave-function characters with respect to the $\{E, (\mathrm{H}_2\ \mathrm{H}_3), E^*, (\mathrm{H}_2\ \mathrm{H}_3)^*\}$ subgroup of D_{3h}(M). This way the parity was recognized and the non-degenerate states were assigned with their D_{3h}(M) irreducible representation labels. To distinguish degenerate states from non-degenerate ones by symmetry, it would also be necessary to evaluate characters of the $(\mathrm{H}_1\ \mathrm{H}_2)$ permutation operator. This is, however, not straightforward in the chosen coordinate system and DVR basis. Fortunately, the degeneracies could mostly be recognized either by energy, when the levels were sufficiently isolated from each other, or by visual inspection of the densities, where the two components of a degenerate level formed a characteristic pair.

Second, labels of not yet assigned states were estimated by a generalized vibrational build-up principle, similar to what we already used in our study of the water molecule,[5] but also taking into account the effect of tunneling and that of the degenerate modes. The appropriate code keeps track of all already assigned labels and, for the currently examined state, suggests the logically closest higher excitations accordingly. The basic idea is that for an n-tuplet of quantum numbers, there is a natural ordering between certain excited states. Let us take a quadruplet of quantum numbers $(v_1\ v_2\ v_3\ v_4)$ as an example. Then, the ground state is (0 0 0 0), by definition. Logically, then, there are four descendant states with the labels (1 0 0 0), (0 1 0 0), (0 0 1 0), and (0 0 0 1), one of which has to be the first excited vibrational state. Each excited state thus has to be followed either by one of its natural descendants or by one of the not yet assigned descendants of earlier assigned states. It is also natural that the following ordering of the states, (0 1 0 0) < (0 1 1 0) < (0 1 2 0) < (1 1 2 5), must be correct, even though there may be other states in between them. When a system exhibits vibrational tunneling, which is the case for ammonia, then each state is split into "+" and "−" components, although the ordering may differ for each state. This makes the general build-up principle complicated as it allows for uneven orderings, such as $(0\ 1\ 2\ 0)^- < (0\ 2\ 2\ 0)^+ < (0\ 1\ 2\ 0)^+ < (0\ 2\ 2\ 0)^-$, although the principle remains strict. The presence of degenerate modes in ammonia requires inclusion of all the irrep labels that come out of their excited-state decompositions (see Secs. II C and II D) into the list of candidate labels for the state under examination. Employing the vibrational build-up principle helps substantially not only to assign complicated highly excited states but also to ensure that no excited-state label is accidentally omitted during the assignment of a large number of states.

Third, comparison and recognition of known density patterns of individual vibrational modes are performed, similar to that already described in our earlier work.[5] The similarities between RDMs are quantified automatically by computing their mutual overlaps. The associated code also keeps track of all the already assigned states and stores their modes' appropriate RDMs as unique patterns corresponding to a particular mode quantum number. All the degenerate modes need to be treated as a single supermode possessing of several RDMs and having a single complex label (see Sec. II D). If there is good match between the RDM of a particular mode and a known pattern (the overlap with one RDM pattern is typically high above 0.9, while much less with all the other patterns), then the mode's label is automatically assigned. Otherwise, the state is marked as 1 with a label not yet known, and it is up to the user to decide, in further steps, about the most feasible label based on hints from the other auxiliary tools or by other reasoning.

The last resort is an assignment tool based on the visualization of the RDMs. Surprisingly, visualization is not needed for the vast majority of the states as the other automatic utility codes do an excellent job, leaving little or no doubt about the labels. Nevertheless, in what follows, we consider the visual inspection of the RDMs as the final decision-making step for all the assignments. In some cases, visual assessment is the only way to decipher skewed poorly converged wave functions when the RDM pattern matching does not provide plausible suggestions. In other cases, by contrast, deciphering the RDM plots can lead to a maze, while the pattern matching suggestions are indisputable. At any rate, the visual inspection of RDMs remains invaluable for revealing the insight into the multidimensional structure of vibrational states.

Practically, the assignment process is executed following a five-step pseudocode:

1. Determine the symmetry, including parity, of all the computed vibrational wave functions.
2. For the state currently examined, starting from the ground state, generate all possible label candidates based on the vibrational build-up principle and in accord with the state's symmetry.
3. For the state currently examined, compare its RDMs with the pool of RDM patterns of states already assigned. Check that the suggested labels also agree with the list of label candidates from step (2). If some of the mode RDMs is not recognized from

the known patterns and the list of label candidates suggests a not yet assigned quantum number for that mode, consider including the state RDM into the pattern pool as a new pattern after approval in step (4).

4. Visually check the RDM plots of the currently examined state and make sure that they correspond to the suggested label candidate from the previous step. If there is no doubt, then do assign the suggested label to the current eigenstate and also update the pool of patterns, if appropriate. Then, take the next eigenstate and go to step (2). If competing label candidates remain or if the visual inspection of the only candidate raises doubts, then the current eigenstate is marked as not yet assigned and the procedure continues with the next eigenstate in step (2).
5. Start again at the ground state and reexamine all the states not yet assigned. By now, the list of label candidates generated for each such state by the vibrational build-up principle is much shorter as many labels have already been assigned to different levels. The pool of RDM patterns is also broader than during the first run, which leads to better matches with the appropriate modal assignments. Each newly suggested assignment for the state is further examined for consistency of energy gaps between + and − tunneling splitting pairs, completeness of family of states with excited degenerate modes (e.g., no state from the family [0, 0+, 1 2 X], where $X \in \{A_1', A_2', 1E', 2E'\}$ is left unassigned), energy, and RDM similarities with related families of states (e.g., states in families [0, 0+, 1 2 X] and [0, 2+, 1 2 X] are related). If necessary, also inspect the eigenstate by other appropriate RDMs (e.g., three-dimensional) to make sure that the assignment is correct. When there is no doubt, the state is assigned with the suggested label; otherwise, it is left unassigned.

To illustrate the algorithm on a concrete example, we describe here how the assignment of the first ten states proceeded (see Table VI and Fig. 3). State No. 1 has + parity, and since there are no visible nodes in its RDM plots, it is assigned as [0, 0+, 0 0 A_1'], and the RDMs are stored as patterns with appropriate modal labels. State No. 2 has unit overlaps with the stored patterns except for the second mode. By visual inspection, by symmetry, and in accord with the build-up principle, the state is assigned with the label [0, 0−, 0 0 A_2''] and the second mode's RDM is stored as the 0− pattern. State No. 3 also has all RDMs with unit overlap to the stored ground state patterns except for the second mode, which is not yet known. The parity is + , and the build-up principle allows only one such label: [0, 1+, 0 0 A_1']. After the clear visual confirmation, the label is assigned to the state and the second mode's RDM is stored as the 1+ pattern. Similarly, but with the opposite parity, state No. 4 is assigned as [0, 1−, 0 0 A_2''], and the second mode's RDM is stored as the 1− pattern. State No. 5 has again not yet recognized RDM for the second mode; otherwise, the other modes have unit overlap with the stored ground state RDMs. From its symmetry and in accord with the build-up principle and the visual assessment, it is labeled [0, 2+, 0 0 A_1']. The second mode's RDM pattern 2+ is again stored. States Nos. 6 and 7 are degenerate with + parity and with the first two modes' RDMs known from the ground state. There are two possible labels for the degenerate modes suggested by the build-up principle: either [0, 0+, 1 0 E'] or [0, 0+, 0 1 E']. By visual inspection and also by mere anticipation that the bending character of the fourth mode results in lower energy than the stretching character of the third mode, the degenerate states are assigned as [0, 0+, 0 1 E_+'] and [0, 0+, 0 1 E_-'], respectively, where we introduce the $_+$ and $_-$ subscripts to distinguish between the two E' states. The RDM patterns 0 1 E_+' and 0 1 E_-' are stored for the combined third and fourth modes since the modes are degenerate and thus need common treatment (see Sec. II D). The pattern matching for states Nos. 8 and 9 yields a direct assignment and labels [0, 0−, 0 1 E_+''] and [0, 0−, 0 1 E_-''], respectively, since all the RDM patterns are already known and these labels are in accord with the build-up principle and also with the visual assessment. No new patterns are needed to be stored. For state No. 10, pattern matching suggests [0, X−, 0 0 A_2'']. The only allowed label of this kind from the build-up principle and also in accord with the visual inspection of the RDMs is [0, 2−, 0 0 A_2'']. The label is thus assigned with the state, and the second mode's RDM is stored as the 2− pattern.

This way, we were able to reliably provide vibrational labels to about 500 of the lowest 600 eigenstates of $^{14}NH_3$.

C. Comparison with CoYuTe assignments

For comparison and an impartial assessment of our results obtained for $^{14}NH_3$, we chose the recent large ammonia high-temperature ro-vibrational line and energy level list known as the CoYuTe[6] list, assembled in 2019. There is an even newer list[32] supplementing the CoYuTe list, but it is amended by an earlier set of results of the present study, so the comparison to that list would not be impartial. The much larger number of states in the CoYuTe[6] list was labeled automatically based on overlaps of the computed wave functions with the FBR basis functions. A comprehensive comparison of our results to the vibrational states of CoYuTe with excitation energies under 10 000 cm^{-1} is shown in the supplementary material. In Table VI, we selected levels relevant for discussion. The ordering of the energy levels in Table VI is dictated by the CoYuTe list.

Most of the energy levels reported by the two studies are as close in energy as a few cm^{-1}. Nevertheless, there are also significant differences, some mentioned below. For the 600 distinct states computed during this work, we can distinguish three blocks. The first block covers the lowest 297 energy levels of the CoYuTe list, which means ~440 distinct states (after counting the two components of degenerate levels separately). Within this block, all the states could be smoothly and unambiguously assigned in this work based on symmetry and the semi-automatic RDM pattern-recognition technique. Apart from subtle differences in energy level orderings, where the energy separation of neighboring states is within a fraction of a cm^{-1} (e.g., level Nos. 40 vs 41, Nos. 42 vs 43, Nos. 48 vs 49, Nos. 51 vs 52, and many others), there are also states with unusually large energy differences between the CoYuTe list and the results of this work. Examples include levels No. 173 or No. 175, which differ by more than 20 cm^{-1} between the two studies, while their neighbors are nicely matched within 2–6 cm^{-1}. Similar examples are levels Nos. 215 and 271. Except for level No. 271 out of the four mentioned, this work provides significantly lower energies than CoYuTe. This can be rationalized by the superior Hamiltonian (we employ an exact Hamiltonian) and basis used during our GENIUSH

computations. The odd result is that level No. 271 is predicted to be as much as 76 cm^{-1} above the CoYuTe energy. If we look into the tunneling splittings of the states instead of their absolute energies, the results of this work match the CoYuTe list very well, the exception is again level No. 271. This state is labeled as [1, 4−, 0 1 E''] and has its tunneling counterpart [1, 4+, 0 1 E'] at level No. 234. The tunneling splitting predicted by CoYuTe is 513 cm^{-1}, which is significantly different from this work's 595 cm^{-1}. Tunneling splittings of other states with the same [·, 4±, ...] pattern are about 600 cm^{-1} in both CoYuTe and this work. Therefore, we believe that the CoYuTe energy of 8937.31 cm^{-1} for level No. 271 is incorrect.

We identified several misassignments in the CoYuTe list in the first block. For example, CoYuTe uses the same label for levels Nos. 88 and 85, while completely omitting the label [0, 0+, 0 four A_1']. Similar label redundance/omitting characterizes the CoYuTe levels Nos. 109 vs 101, Nos. 110 vs 102, Nos. 216 vs 219, Nos. 222 vs 200, and Nos. 223 vs 202. For levels Nos. 139 and 143, the labeling is swapped with respect to results of this work. For levels Nos. 195, 196, 201, 203, 204, 205, 212, and 286, the CoYuTe list exhibits a bit more complicated misassignments. Here, we discuss only level No. 195, labeled by CoYuTe as [1, 0+, 1 1 $A_2'(1\ 1)$]. The reasoning employed for the other states can be understood from Table VI. The label of level No. 195 suggested by CoYuTe is assigned during this work for level No. 222. For that level, in turn, CoYuTe suggests the label [0, 0+, 1 3 A_2']. However, that has already been assigned to level No. 200 by both CoYuTe and this work. Moreover, CoYuTe does not have the label [1, 0+, 0 3 A_2'] listed, which is assigned to level No. 195 in our work. This means that the CoYuTe assignment protocol did not succeed to predict these few cases correctly, while our labels remain consistent and complete.

The second block of states involves levels Nos. 298–360. Contrary to the first block, not all the states could be assigned unambiguously by the RDM method. States assigned during this work match their CoYuTe counterparts, except level No. 328 whose CoYuTe assignment is odd (the CoYuTe label [1, 0−, 0 4 A_2'' (0 0)] is missing its tunneling counterstate [1, 0+, 0 4 $A_1'(0\ 0)$], and also the [0, 0−, 0 6 A_2'' (0 0)] label is missing). The other CoYuTe labels within the second block agree with the RDM-based predictions; nevertheless, due to ambiguities in RDM patterns, such states were left unassigned during this work. In this block, there are still many CoYuTe energy levels that are close to those predicted by this work, but an increasing number of levels differ significantly.

In the remaining, third block of states, starting from energy level No. 361, there are only a few states that are reliably assigned by the RDM method. Most of the states could not even be matched by energy and symmetry between the CoYuTe list and the results of this work. Such states are left out from comparison and put at the very end of the table for reference. In order to assign more states reliably, a larger basis set and better convergence of the highly excited wave functions need to be achieved. The auxiliary codes would also need more development in ranking the plausible label candidates by estimating their energy according to earlier assigned levels and tunneling splittings of similarly excited labels. The differences in symmetry of the remaining unmatched states between the CoYuTe list and the states predicted in this study suggest that at such high energies, the results are sensitive to the qualityof the computations, which can lead to a considerable shuffle of states ordering.

V. CONCLUSIONS

We demonstrated, on the example of the ammonia ($^{14}NH_3$) molecule, that the use of reduced-density matrices helps to achieve a thorough understanding of the multidimensional structure of non-trivial excited vibrational wave functions. The reduced-density matrix approach is not only limited to using normal coordinates but also particularly suitable for systems described by arbitrary internal coordinates. The vibrational assignment process based on RDMs and internal coordinates had already been employed for the vinyl radical[4] and the water molecule.[5] The ammonia molecule used in the present study represents a substantially more complex system as it not only exhibits internal tunneling motion but also possesses two degenerate interacting vibrational modes. To succeed, we had to reformulate the conventional treatment and labeling of systems with several degenerate modes (the method of vibrational angular momenta, which is commonly used to describe ammonia vibrations, does not respect molecular symmetry, cannot predict correct degeneracy, and prevents full understanding of mutual inter-state relations). The result is a general, unique, and insightful labeling scheme that respects the system's symmetry.

With the RDM algorithm developed, we were able to correctly assign several 100 vibrational states of ammonia with relative ease. Our study also confirms that excited vibrational states tend to have a truly modal structure, i.e., the multidimensional wave function is decomposable to individually excited modes to a good degree of approximation. Reduced-density matrices representing particular excited vibrational modes are very characteristic and can serve as reliable patterns for a quick and semi-automatic state assignment. Moreover, the visual representation of the various RDMs gives an invaluable insight into the physical meaning of the excited modes and their mutual relations.

The RDM method presented, together with the reformulated treatment of excited degenerate modes and through the auxiliary codes developed, represents a cutting-edge technique for revealing and understanding the internal structure of excited multidimensional vibrational states. The method is applicable to arbitrary (Abelian or non-Abelian) molecular systems for which excited vibrational wave functions can be practically computed so that the nodal structure significant to a particular vibrational motion can be examined. For large molecules, it may also mean that at least a portion of the PES that is related to a specific vibrational motion is available. The RDM algorithm developed is a significantly improved alternative to basis-set-decomposition-based assignment approaches.

Finally, we note that after comparing our results to the large, recently published CoYuTe[6] list of vibrational states of ammonia, we identified several misassignments and inconsistencies in the CoYuTe list.

SUPPLEMENTARY MATERIAL

See the supplementary material for a complete version of Table VI comparing vibrational states of ammonia from the CoYuTe[6] list with the results of this work.

ACKNOWLEDGMENTS

The work performed in Budapest received support from the NKFIH (Grant No. K119658) and from the ELTE Institutional Excellence Program (Grant No. TKP2020-IKA-05) financed by the Hungarian Ministry of Human Capacities (EMMI). Computational resources used in Prague were supplied by the project "e-Infrastruktura CZ" (e-INFRA LM2018140) provided within the program Projects of Large Research, Development and Innovations Infrastructures. The authors are grateful to Professor Sergey Yurchenko for useful discussions and comments.

DATA AVAILABILITY

The data that support the findings of this study are available within the article and its supplementary material.

REFERENCES

[1] A. G. Császár, C. Fábri, T. Szidarovszky, E. Mátyus, T. Furtenbacher, and G. Czakó, "Fourth age of quantum chemistry: Molecules in motion," Phys. Chem. Chem. Phys. **14**, 1085–1106 (2012).

[2] E. Mátyus, C. Fábri, T. Szidarovszky, G. Czakó, W. D. Allen, and A. G. Császár, "Assigning quantum labels to variationally computed rotational-vibrational eigenstates of polyatomic molecules," J. Chem. Phys. **133**, 034113 (2010).

[3] G. Hose and H. S. Taylor, Phys. Rev. Lett. **51**, 947 (1983).

[4] J. Šmydke, C. Fábri, J. Sarka, and A. G. Császár, "Rovibrational quantum dynamics of the vinyl radical and its deuterated isotopologues," Phys. Chem. Chem. Phys. **21**, 3453–3472 (2019).

[5] J. Šmydke and A. G. Császár, "On the use of reduced-density matrices for the semi-automatic assignment of vibrational states," Mol. Phys. **117**, 1682–1693 (2019).

[6] P. A. Coles, S. N. Yurchenko, and J. Tennyson, "ExoMol molecular line lists–XXXV. A rotation-vibration line list for hot ammonia," Mon. Not. R. Astron. Soc. **490**, 4638–4647 (2019).

[7] C. C. J. Roothaan, "New developments in molecular orbital theory," Rev. Mod. Phys. **23**, 69 (1951).

[8] E. B. Wilson, Jr., J. C. Decius, and P. C. Cross, *Molecular Vibrations* (McGraw-Hill, New York, 1955).

[9] J. N. Murrell, S. Carter, S. C. Farantos, P. Huxley, and A. J. C. Varandas, *Molecular Potential Energy Surfaces* (Wiley, New York, 1984).

[10] P. G. Mezey, *Potential Energy Hypersurfaces* (Elsevier, New York, 1987).

[11] A. G. Császár, W. D. Allen, Y. Yamaguchi, and H. F. Schaefer, "*Ab initio* determination of accurate ground electronic state potential energy hypersurfaces for small molecules," in *Computational Molecular Spectroscopy* (Wiley, New York, 2000), pp. 15–68.

[12] M. S. Child and L. Halonen, "Overtone frequencies and intensities in the local mode picture," Adv. Chem. Phys. **57**, 1–58 (1984).

[13] S. N. Yurchenko, W. Thiel, and P. Jensen, "Theoretical rovibrational energies (trove): A robust numerical approach to the calculation of rovibrational energies for polyatomic molecules," J. Mol. Spectrosc. **245**, 126–140 (2007).

[14] T. Mathea and G. Rauhut, "Assignment of vibrational states within configuration interaction calculations," J. Chem. Phys. **152**, 194112 (2020).

[15] M. Gruebele, "Intensities and rates in the spectral domain without eigenvectors," J. Chem. Phys. **104**, 2453–2456 (1996).

[16] H.-G. Yu, H. Song, and M. Yang, "A rigorous full-dimensional quantum dynamics study of tunneling splitting of rovibrational states of vinyl radical C_2H_3," J. Chem. Phys. **146**, 224307 (2017).

[17] A. G. Császár, E. Mátyus, T. Szidarovszky, L. Lodi, N. F. Zobov, S. V. Shirin, O. L. Polyansky, and J. Tennyson, "First-principles prediction and partial characterization of the vibrational states of water up to dissociation," J. Quant. Spectrosc. Radiat. Transfer **111**, 1043–1064 (2010).

[18] D. A. Sadovskiĭ, N. G. Fulton, J. R. Henderson, J. Tennyson, and B. I. Zhilinskiĭ, "Nonlinear normal modes and local bending vibrations of H_3^+ and D_3^+," J. Chem. Phys. **99**, 906–918 (1993).

[19] J. Sarka and A. G. Császár, "Interpretation of the vibrational energy level structure of the astructural molecular ion H_5^+ and all of its deuterated isotopomers," J. Chem. Phys. **144**, 154309 (2016).

[20] R. Dawes, X.-G. Wang, A. W. Jasper, and T. Carrington, "Nitrous oxide dimer: A new potential energy surface and rovibrational spectrum of the nonpolar isomer," J. Chem. Phys. **133**, 134304 (2010).

[21] P. R. Bunker and P. Jensen, *Molecular Symmetry and Spectroscopy* (NRC, Ottawa, 1998).

[22] K. Chubb, P. Jensen, and S. Yurchenko, "Symmetry adaptation of the rotation-vibration theory for linear molecules," Symmetry **10**, 137 (2018).

[23] L. Tisza, Z. Phys. **82**, 48 (1933).

[24] M. Hamermesh, *Group Theory and Its Application to Physical Problems* (Addison-Wesley, Reading, MA, 1962).

[25] A. G. Császár, "Anharmonic force field of CO_2," J. Phys. Chem. **96**, 7898–7904 (1992).

[26] E. Mátyus, G. Czakó, and A. G. Császár, "Toward black-box-type full- and reduced-dimensional variational (ro)vibrational computations," J. Chem. Phys. **130**, 134112 (2009).

[27] C. Fábri, E. Mátyus, and A. G. Császár, "Rotating full- and reduced-dimensional quantum chemical models of molecules," J. Chem. Phys. **134**, 074105 (2011).

[28] Z. Bacic and J. C. Light, Annu. Rev. Phys. Chem. **40**, 469 (1989).

[29] J. C. Light and T. Carrington, "Discrete-variable representations and their utilization," in *Advances in Chemical Physics* (John Wiley & Sons, Inc., 2007), pp. 263–310.

[30] C. Lanczos, J. Res. Natl. Bur. Stand. **45**, 255 (1950).

[31] S. N. Yurchenko, R. J. Barber, J. Tennyson, W. Thiel, and P. Jensen, "Towards efficient refinement of molecular potential energy surfaces: Ammonia as a case study," J. Mol. Spectrosc. **268**, 123–129 (2011).

[32] T. Furtenbacher, P. A. Coles, J. Tennyson, S. N. Yurchenko, S. Yu, B. Drouin, R. Tóbiás, and A. G. Császár, "Empirical rovibrational energy levels of ammonia up to 7500 cm^{-1}," J. Quant. Spectrosc. Radiat. Transfer **251**, 107027 (2020).